Rapid Communications

Droplets on chemically patterned surface: A local free-energy minima analysis

Yanchen Wu* and Fei Wang†
Institute of Applied Materials–Computational Materials Science, Karlsruhe Institute of Technology, Straße am Forum 7, 76131 Karlsruhe, Germany

Michael Selzer and Britta Nestler
Institute of Applied Materials–Computational Materials Science, Karlsruhe Institute of Technology, Straße am Forum 7, 76131 Karlsruhe, Germany
and Institute of Digital Materials Science, Karlsruhe University of Applied Sciences, Moltkestraße 30, 76133 Karlsruhe, Germany

(Received 24 June 2019; published 24 October 2019)

Droplet wetting on solid surfaces is a ubiquitous phenomenon in nature and applications. The wetting behavior of droplets on homogeneous surfaces has been accurately elucidated by the quintessential Young's law. However, on heterogeneous substrates, due to the energy barriers and contact line pinning effect, more than one equilibrated droplet pattern exists, which is more close to reality. Here, we propose a concise mathematical-physical model to delineate the droplet patterns on chemically patterned surfaces: stripe, "chocolate," and "chessboard." The present concept is capable of predicting the number as well as the morphologies of the equilibrated droplets on chemically patterned surfaces. We anticipate that the current work can be applied to fabricate programmable surfaces involving droplet manipulation in integrated circuits, biochips, and smart microelectronics.

DOI: 10.1103/PhysRevE.100.041102

The wetting of droplets on a solid substrate is omnipresent in nature [1]. When the substrate is homogeneous, the equilibrium shape of the droplet is unique, as predicted by the classic Young's law [2–4]. However, in most technological and engineering applications [5–11], the substrate is presumably heterogeneous. The heterogeneities of the surfaces most probably lead to various local energy minima [12–25], corresponding to multiple equilibrium droplet morphologies. In such an intricate case, neither the Young's law nor the classic Cassie-Baxter model [26] is sufficient to describe the equilibrated droplet patterns. In contrast to a unique droplet shape on homogeneous substrates, droplet morphologies on heterogeneous substrates, which provide more appealing freedom for droplet manipulation as well as design of programmable surfaces in applications, are far from being understood.

In this work, we propose a concise mathematical-physical model to address the droplet patterns on chemically patterned surfaces. Three typical heterogeneous substrates, namely, stripe, "chocolate," and "chessboard" (Fig. 1), are contemplated. Our concept is based on the physical principle of surface energy minimization, following the second law of thermodynamics. The present model creates a way to recount the potential existing equilibrated droplet patterns on flat and chemically patterned surfaces based on a finite dimensional energy landscape. The results of our model show good conformity with the phase-field simulations.

We consider a sessile droplet on a chemically patterned solid surface surrounded by a gas phase, as illustrated in Fig. 1. The droplet arrives at the equilibrium state by minimizing the total interfacial energy $E = A_{\mathrm{lg}}\gamma_{\mathrm{lg}} + \int_{A_{\mathrm{ls}}}(\gamma_{\mathrm{ls}} - \gamma_{\mathrm{gs}})dA$. Here, A_{lg} and A_{ls} denote the areas of the liquid-gas and liquid-solid interfaces, respectively. The parameters γ_{lg}, γ_{ls}, and γ_{gs} indicate the liquid-gas, liquid-solid, and gas-solid interfacial and surface energies, respectively. It is assumed that the droplet baseline (red dashed line) forms an ellipse with semiaxes a and b. The liquid-gas interface is described with circular arcs (yellow dashed line) passing through the droplet apex and the contact line. These circular arcs have a varying curvature radius $r_c(\varphi) = [r_b^2(\varphi) + h^2]/2h$, where r_b, h, and φ are the base radius, droplet height, and polar angle of the base ellipse, respectively. Mathematically, the area of the droplet cap (i.e., the liquid-gas interface) A_{lg} can be fully described by a, b, and h. For a given volume $V_d(a, b, h)$, A_{lg} is further reduced to be a function with two degrees of freedom, i.e., $A_{\mathrm{lg}} = A_{\mathrm{lg}}(a, b)$. Thus, the first term of the total interfacial energy is $\gamma_{\mathrm{lg}}A_{\mathrm{lg}} = E_1(a, b)$. For convenience, we set γ_{lg} a dimensionless value $\gamma_{\mathrm{lg}} = 1$.

The chemical heterogeneities of the solid surface $\gamma_{\mathrm{ls}} - \gamma_{\mathrm{gs}} = f_k(r_b, \varphi)$ ($k = 1, 2, 3$ denote the striped, chocolate, and chessboard patterns, respectively) are described as follows:

$$\gamma_{\mathrm{ls}} - \gamma_{\mathrm{gs}} = \begin{cases} f_1(r_b, \varphi) = \gamma_m + \gamma_0 \tanh(\xi \cos\delta_1), & \text{striped pattern} \\ f_2(r_b, \varphi) = \gamma_m + \gamma_0 \tanh[\xi(\cos\delta_1 \cos\delta_2 - \cos\delta_1 - \cos\delta_2)], & \text{chocolate pattern} \\ f_3(r_b, \varphi) = \gamma_m + \gamma_0 \tanh(\xi \cos\delta_1 \cos\delta_2), & \text{chessboard pattern} \end{cases} \quad (1)$$

*yanchen.wu@kit.edu
†fei.wang@kit.edu

with $\delta_1 = [\pi r_b \sin\varphi + i\pi L]/L$ and $\delta_2 = [\pi r_b \cos\varphi + j\pi L]/L$. γ_m and γ_0 are the mean surface energy difference and the amplitude of the heterogeneity, respectively. Presently, we set $\gamma_m = 0$, $\gamma_0 = 0.5$, i.e., the static equilibrium contact angles on the hydrophilic and hydrophobic areas are 60° and 120°, respectively. The characteristic length L denotes the width of the stripe for the striped pattern and the lattice length for the chocolate and chessboard patterns. ξ is a constant parameter controlling the sharpness of the chemical pattern and $i, j = 0, \pm1, \pm1/2,...$ are parameters depicting the center point position of the droplet baseline, which will be specified in the following. The interfacial energy of the liquid-solid interface has four degrees of freedom, namely, $\int_{A_{ls}} (\gamma_{ls} - \gamma_{gs}) dA = E_2(a, b, i, j)$. For a certain patterned surface and droplet position (i.e., for certain values of i, j), E_2 can be described as a function of a and b. The equilibrium droplet shapes are predicted by minimizing the total interfacial energy E in terms of a and b when i, j are fixed. A detailed discussion about the influence of i, j for given parameters a and b is elucidated in the Supplemental Material [27].

To capture the complex morphologies of droplets on chemically patterned surfaces and their relaxation into equilibrium shapes, an Allen-Cahn-type phase-field model (PFM) is employed [28,29]. This is a computationally efficient method for solving wetting phenomena, which has been experimentally validated [30,31]. In the PFM, the phase state is characterized by a continuous space and time dependent order parameter $\phi(x, t)$. The time evolution of this order parameter is such as to reduce the free-energy functional, which is expressed as

$$F = \int_V \left[\frac{1}{\varepsilon} w(\phi) + g(\phi) + \varepsilon \gamma_{lg} |\nabla \phi|^2 \right] dV. \tag{2}$$

Here, V is the spatial domain and ε is a modeling parameter related to the thickness of the liquid-gas interface. The first term $w(\phi)$ is an obstacle potential, which is written as $w(\phi) = (16/\pi^2)\gamma_{lg}\phi(1-\phi)$, if $\phi \in [0, 1]$ and $w(\phi) = \infty$, if $\phi \notin [0, 1]$ (see Ref. [28]). The second term $g(\phi)$ is to ensure the volume preservation [28,29]. The last contribution $\varepsilon\gamma_{lg}|\nabla\phi|^2$ denotes a gradient energy density. In order to fulfill the wetting condition, a solid-fluid interfacial energy density f_w is added to the free energy F, such that $F_{total} = F + \int_{A_{ls}} f_w(\phi) dA$. Here, $f_w = \gamma_{gs} h(\phi) + \gamma_{ls}[1 - h(\phi)]$ is a wall free-energy density [30], where $h(\phi)$ is an interpolation function. Through the functional derivative of F_{total}, the evolution equation for the phase order parameter reads

$$\tau\varepsilon\partial_t\phi = 2\varepsilon\gamma_{lg}\Delta\phi - g'(\phi) - \frac{16}{\varepsilon\pi^2}\gamma_{lg}(1-2\phi) \quad \text{in } V, \tag{3}$$

with the natural boundary condition [32,33]:

$$2\varepsilon\gamma_{lg}\partial_n\phi = (\gamma_{gs} - \gamma_{ls})h'(\phi) \quad \text{on } A_{ls}. \tag{4}$$

Here, τ in Eq. (3) is a relaxation parameter. In Eq. (4), n denotes the normal vector of the solid-fluid boundary A_{ls}. At equilibrium, this boundary condition leads to the Young's law.

We now present the analytical predictions and simulation results of droplets on a chemically striped patterned surface

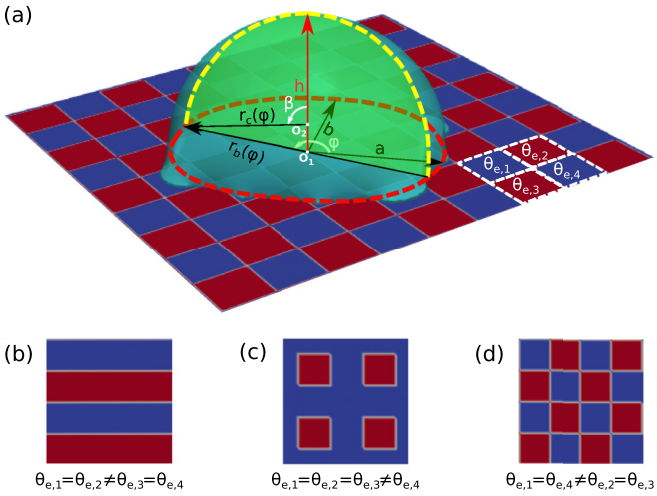

FIG. 1. (a) A sessile droplet on chemically patterned surface. The dashed ellipse (with center O_1 semiaxes a and b) is the droplet baseline. The dashed circular arc is on the liquid-gas interface with the circle center O_2 and curvature radius r_c. β depicts the polar angles on the surface of the yellow dashed arc. $\theta_{e,1}$ to $\theta_{e,4}$ describe the intrinsic contact angles on the pattern lattices. (b)—(d) Selected chemically patterned surfaces: stripe, "chocolate," and "chessboard," defined by the arrangement of the intrinsic contact angles.

[see Fig. 1(b)]. In Figs. 2(a)–2(c), we illustrate the surface energy landscapes of droplets in terms of the parameters a and b as well as the corresponding snapshots of the equilibrated droplets via PFM. In the simulations, the droplets with a given volume initially have a form of cuboid with various aspect ratios in the contact area. Suitable aspect ratios and initial positions of the droplets are chosen (see Supplemental Material [27]), such that the surface energy minima predicted by the analytical model can be reached. As shown in the first picture of Fig. 2(a)(III), a and b are the semiaxes of the elliptic baseline of droplets, which are parallel and perpendicular to the stripes, respectively. The surface energy minima indicated by different numbers in the energy diagrams correspond to the snapshots labeled with the same number. The effective droplet radii $R = (3V_d/4\pi)^{1/3}$ in Figs. 2(a), 2(b) and 2(c) are 40, 50, and 90, respectively. The blue and red stripes in the snapshots denote the hydrophilic and hydrophobic ones with the same stripe width $L = 20$. In Fig. 2(a)(III), the red dashed ellipses denote the analytical results, corresponding to the coordinate of the energy minimum points in the energy diagrams. A good agreement is observed between the analytical solution and the numerical simulations and three equilibrated droplets are found. Similarly, as illustrated in Figs. 2(b) and 2(c), 4 and 5 equilibrium shapes are found for the droplets with $R = 50$ and $R = 90$, respectively. By using the same methods, we obtain droplet configurations for different droplet sizes, as depicted in Fig. 2(d), where the ratio R/L ranges from 2 to 9. Both the number of the equilibrium shapes and the tendency of the analytical results show a satisfactory agreement with the simulation results. Because of the contact line pinning in the direction perpendicular to the stripes, the value of b is well predicted by the analytical model. However, for large a, the analytical predictions of a deviate from the simulations, which is caused by the assumption of the analytical model

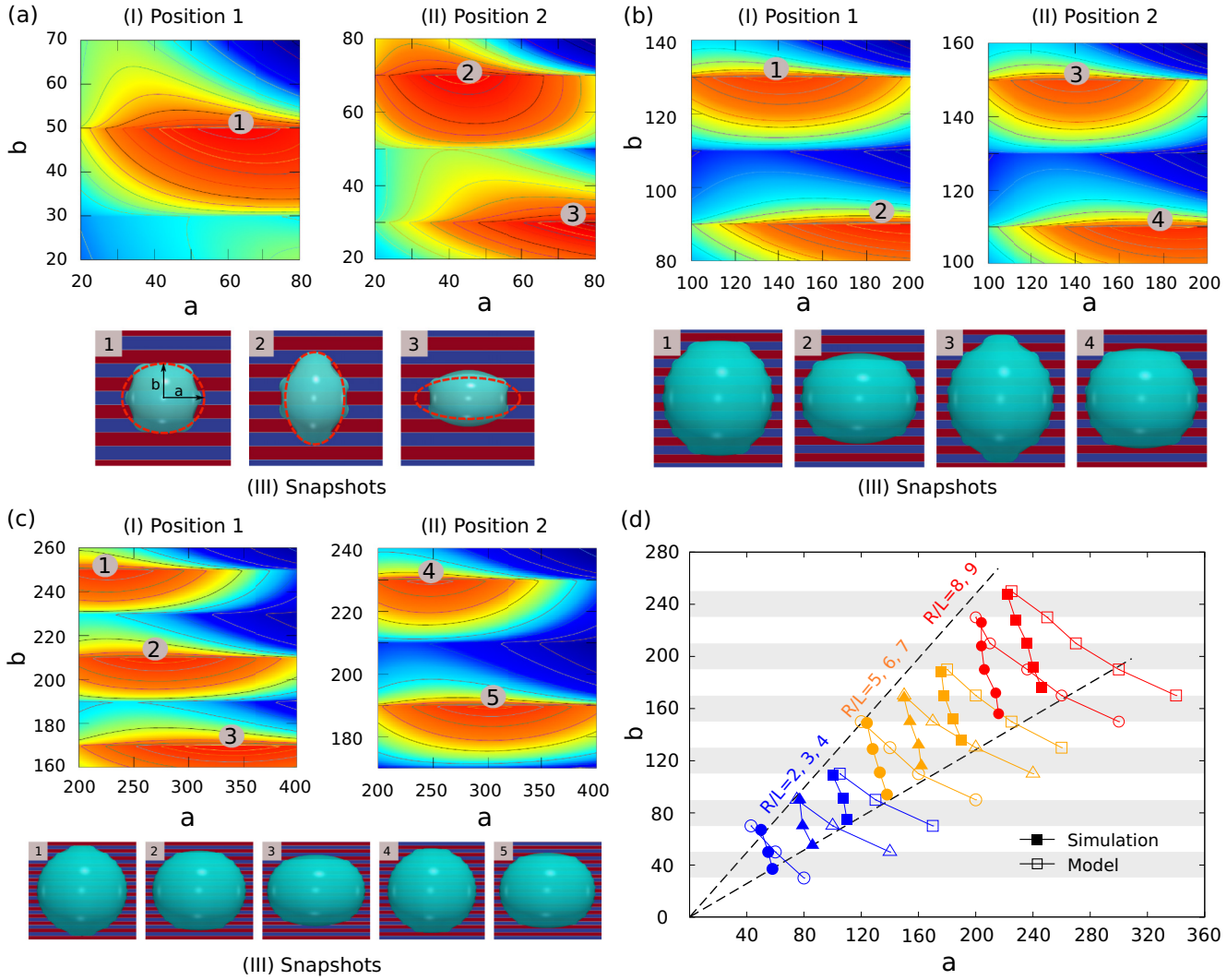

FIG. 2. (a)–(c) Surface energy landscapes in the a-b space and snapshots of sessile droplets on chemically striped patterned surfaces with different droplet sizes [(a) $R/L = 2$, (b) $R/L = 5$, (c) $R/L = 9$]. The chemical heterogeneities are described by $f_1(r_b, \varphi)$ in Eq. (1). At equilibrium, the droplet base center stays either on the center of the blue (hydrophilic) stripe (namely, position 1 and $i = 1$) or on the center of the red (hydrophobic) one (i.e., position 2 and $i = 0$). The energy landscapes are accordingly calculated when the droplet base centers are on these two different positions. The contour lines indicate the energy levels (red for low energy and blue for high energy states) and the color changes from blue to red illustrate the decrease of the energy. The energy minima are indicated by different numbers, corresponding to the snapshots labeled with the same number. The red dashed ellipses in (a)(III) denote the analytical results, which can be read from the corresponding energy landscapes. (d) Predicted droplet configurations for different droplet sizes. The filled and empty symbols describe the simulation and analytical results, respectively. The two dashed lines are guide lines to highlight a trend in the data.

that the liquid-gas interface is described with circular arcs; while this is obviously not the case when the droplet aspect ratio a/b is relatively large and the deformation of the contact lines takes an important role. From Fig. 2(d), we conclude that the number of the equilibrium droplet shapes (or the local energy minima) remains constant as the droplet volume increases within a certain range (e.g., $R/L = 2, 3, 4$), while a further rise of the droplet volume results in an increase in the number of equilibrium droplets (e.g., from $R/L = 4$ to $R/L = 5$).

Afterwards, a two-dimensional periodic solid surface pattern, the chocolate pattern, is considered [see Fig. 1(c)]. In this pattern, the size of the lattices and the distance between them both are set to be 20. The effective droplet radius is $R = 40$. In the simulations, the droplets initially have a cuboid form with different aspect ratios and then evolve to equilibrium shapes. Figures 3(a)–3(c) show the surface energy landscapes for droplets with the base center points on P_1 ($j = 0, i = 0$), P_2 ($j = 1, i = 0$), and P_3 ($j = 1, i = -1$), respectively [see Fig. 3(d)]. Figure 3(e) illustrates the simulation results of the equilibrium shapes of droplets. The energy minima indicated by different numbers correspond to the snapshots in Fig. 3(e) labeled with the same number. The red dashed ellipses in Fig. 3(e) are the analytical predictions, which show good agreement with the simulation results. It is found that the energy diagrams (a) and (c) are symmetric with

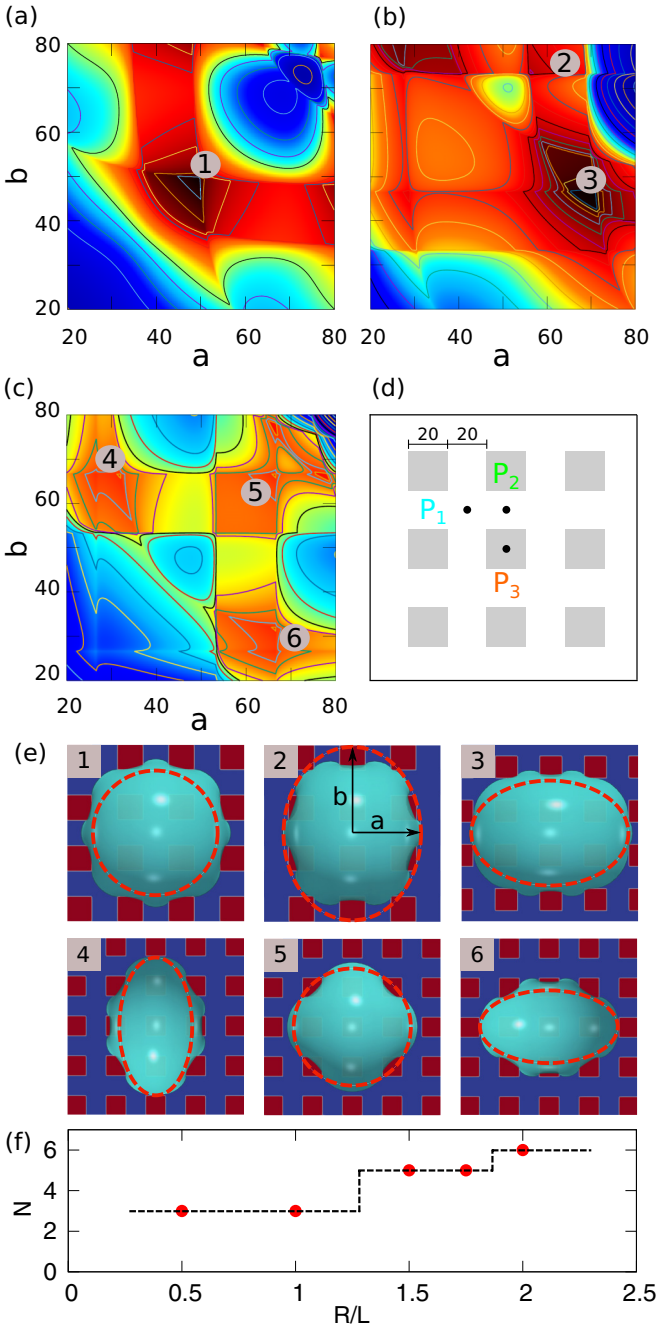

FIG. 3. (a)–(c) Surface energy landscapes for chocolate-patterned surfaces. The chemical heterogeneities are described by $f_2(r_b, \varphi)$ in Eq. (1). The energy minima are indicated by different numbers, corresponding to the snapshots in (e) labeled with the same number. (d) Sketch of the surface topology and three base centers of droplets (gray, hydrophobic; white, hydrophilic). The droplet shapes in (a), (b), and (c) correspond to the positions P_1, P_2, and P_3. (e) Snapshots of equilibrated droplets through PFM (blue, hydrophilic; red, hydrophobic). The red dashed ellipses denote the analytical results. (f) The number N of equilibrium shapes of droplets as a function of R/L. The black dashed line is the guide line.

respect to the line $a = b$, while in (b) this symmetric characteristic disappears. This is because the topologies in a and b directions are the same for the points P_1 and P_3, while for the point P_2 the topologies vary in the two directions. In comparison to the droplets with the same size ($R = 40$) on the striped patterned, more local energy minima are found for droplets on the chocolate-patterned surface. Furthermore, by changing the droplet volume, we have found a functional relation between the number of equilibrium shapes of droplets N and the droplet size R/L, as illustrated in Fig. 3(f). The red points indicate the predicted values of N for different R/L. The black dashed line highlights the functional tendency, showing that larger droplets tend to have more equilibrium patterns.

We further utilize the analytical model and PFM to scrutinize the equilibrated droplets on a more complex pattern, the chessboard pattern [see Fig. 1(d)]. The effective droplet radius is $R = 40$ and the lattice length of the chessboard is $L = 20$. Figures 4(a) and 4(d) show the energy landscapes for droplets deposited on the positions P_1 ($j = 0, i = 0$) and P_2 ($j = 0, i = 1$), respectively. Figures 4(b), 4(c) and 4(e), which is achieved by rotating the coordinate system by 45° [the directions of a and b are shown in Fig. 4(g)5], illustrate the energy landscapes corresponding to the positions P_1, P_3 ($j = -1/2, i = 1/2$), and P_2, respectively. It is found that the analytical predictions [red dashed ellipses in Fig. 4(g)] match very well with the PFM simulations. With the aid of the present model, 11 equilibrated droplet patterns are found for the chessboard-patterned surface with the initial setup $R = 40$ and $L = 20$. The number N of equilibrium shapes of droplets as a function of the droplet size R/L is displayed in Fig. 4(h). The results reveal that the increase in the droplet size leads to more equilibrium shapes of droplets. Currently, we focus on the equilibrium features of droplets on the chemically patterned surface and the capabilities of the analytical model. Systematic studies of parameters such as contact angles will be presented in a future work.

Figure 5 illustrates how the complexity of the pattern influences the number of equilibrated droplets. Here, we introduce a parameter, energy discontinuous line density ρ (see the caption in Fig. 5), to characterize the complexity of the pattern. From striped patterned surface to chocolate-patterned and chessboard-patterned surface, the density of the energy discontinuous line rises, which increases the complexity of the energy landscape [e.g., see energy landscapes in Figs. 2(a), 3, and 4] and thus leads to more and more equilibrated droplets. This increase tendency is more pronounced for larger droplets ($R/L = 2$) than for smaller ones ($R/L = 1.5$ and 0.5). The underlying reason is that more energy discontinuous lines are covered by the large droplets and therefore more stable states tend to occur, whereas for small droplets, the number of covered discontinuous lines is relatively reduced and the equilibrated states are not as many as that for large droplets.

To conclude, we have presented a strategy for delineating the equilibrated droplet patterns on programmable chemically patterned surfaces via calculating the surface energy landscapes. We have applied and validated the strategy by studying equilibrium shapes of droplets on three selected substrate patterns. Together with numerical simulations, we have found the potential existing energy minima and the corresponding equilibrium droplet shapes, while this is not possible by the Cassie-Baxter model. It has been revealed that the increase in the droplet volume or the complexity of the surface (e.g., by introducing more hydrophilic-hydrophobic boundary lines) most likely gives rise to more surface energy minima. Hence,

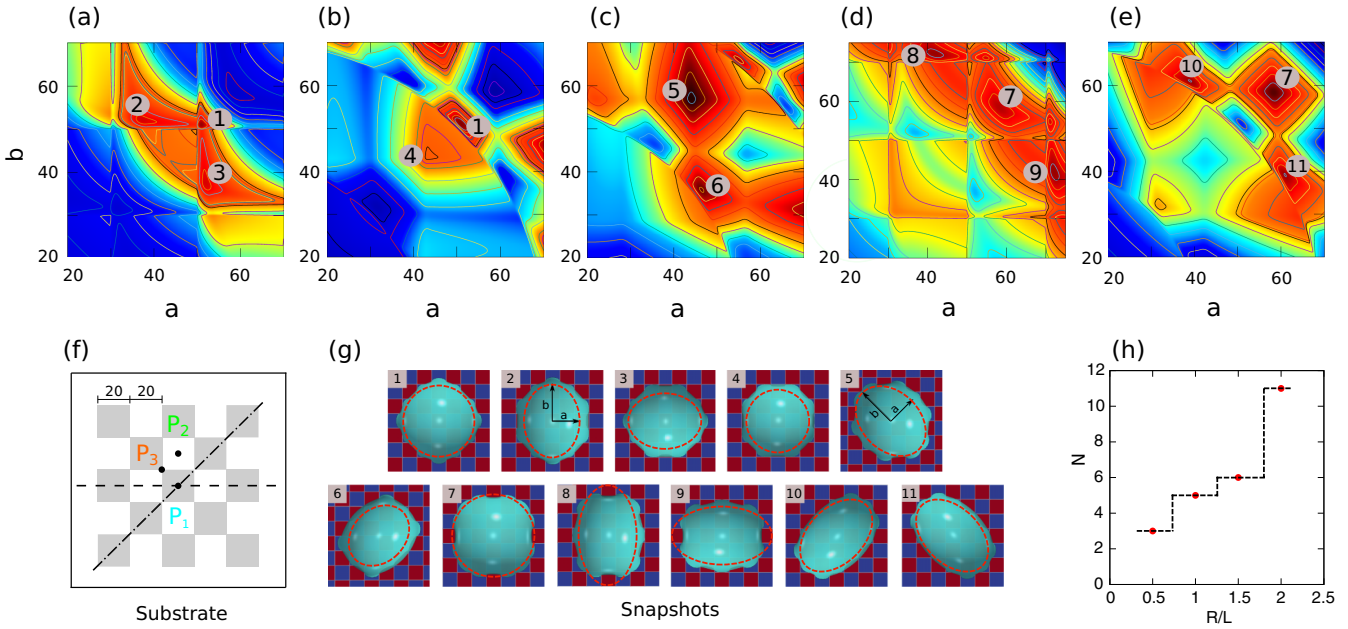

FIG. 4. (a)–(e) Surface energy landscapes for chessboard-patterned surfaces. (a) and (d) correspond to the situations when the directions of a and b are horizontal and vertical, respectively, as shown in (g)2. The chemical heterogeneities are described by $f_3(r_b, \varphi)$ in Eq. (1). (b), (c), and (e) describe the energy landscapes in a rotated coordinate system and the directions of a and b are shown in (g)5. In the rotated system, δ_1 and δ_2 in $f_3(r_b, \varphi)$ are substituted by δ_1' and δ_2', respectively, with $\delta_1' = (\delta_1 + \delta_2)/\sqrt{2}$ and $\delta_2' = (\delta_1 - \delta_2)/\sqrt{2}$. The energy minima are indicated by different numbers, corresponding to the snapshots in (g) labeled with the same number. (f) Schematic description of the surface topology and three base center points of equilibrated droplets (gray, hydrophobic; white, hydrophilic). The two lines indicate two possible directions of the semiaxis a. (a) and (b), (d) and (e), and (c) correspond to P_1, P_2, and P_3, respectively. (g) Snapshots of equilibrated droplets via PFM (blue, hydrophilic; red, hydrophobic). The red dashed ellipses denote the analytical results. (h) The number N of equilibrium shapes of droplets as a function of R/L. The black dashed line is the guide line.

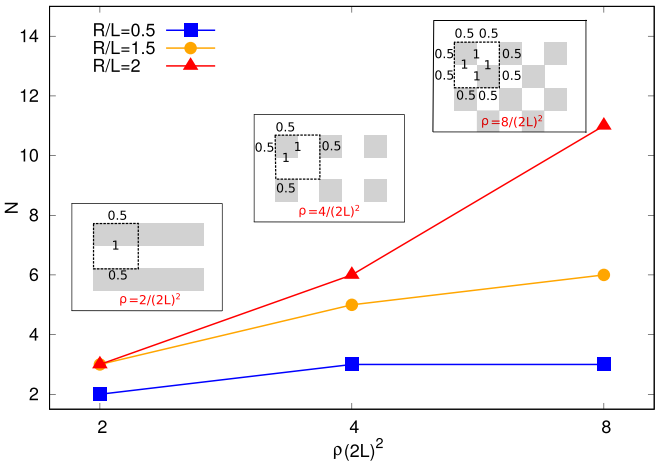

FIG. 5. The number N of equilibrium droplet shapes as a function of the energy discontinuous line density $\rho := n/(2L)^2$ for different patterned surfaces, Here, n is the total effective number of pinning lines within a square cell with an area of $(2L)^2$. The three insets indicate how ρ is calculated for different patterned surfaces. The numbers "1" and "0.5" shown in the cells stand for the effective number of pinning lines. The lines with different symbols denote the results for droplets with different sizes (square, $R/L = 0.5$; circle, $R/L = 1.5$; triangle, $R/L = 2$).

numerous droplet patterns can be quantitatively obtained by tuning the droplet volume or the morphologies of the surfaces. This new insight paves an alternative way to better understand wetting behaviors on chemically patterned surfaces. Our approach can be straightforwardly extended to study droplets deposited on a variety of chemically patterned surfaces and offers essential guidelines for a vast range of applications in microfluidics, inkjet printing, and biomedical science [34,35]. However, on real heterogeneous surfaces, the contact line is highly nonlinear and far more complex than the present approximation of an ellipse. In this case, an infinitely dimensional Fourier series should be adopted to depict the triple line, which gives rise to an infinitely dimensional energy landscape. To find the complete set of the local energy minima in such an infinitely dimensional energy landscape is challenging and cannot be achieved by the present model.

The authors gratefully acknowledge funding of the research through the Gottfried-Wilhelm Leibniz prize NE 822/31-1 of the German Research Foundation (DFG) (DE). Aspects of modeling wetting behavior on a structured surface, integrated in the present Rapid Communication, have been discussed within the VirtMat project of the Helmholtz Association.

[1] A. R. Parker and C. R. Lawrence, Nature (London) **414**, 33 (2001).

[2] P.-G. De Gennes, F. Brochard-Wyart, and D. Quéré, *Capillarity and Wetting Phenomena: Drops, Bubbles, Pearls, Waves* (Springer Science & Business Media, Berlin, 2013).

[3] É. Ruiz-Gutiérrez, J. H. Guan, B. Xu, G. McHale, G. G. Wells, and R. Ledesma-Aguilar, Phys. Rev. Lett. **118**, 218003 (2017).

[4] T. Young, Philos. Trans. R. Soc. London **95**, 65 (1805).

[5] L. Zhai, M. C. Berg, F. C. Cebeci, Y. Kim, J. M. Milwid, M. F. Rubner, and R. E. Cohen, Nano Lett. **6**, 1213 (2006).

[6] H. Bai, L. Wang, J. Ju, R. Sun, Y. Zheng, and L. Jiang, Adv. Mater. **26**, 5025 (2014).

[7] K.-C. Park, P. Kim, A. Grinthal, N. He, D. Fox, J. C. Weaver, and J. Aizenberg, Nature (London) **531**, 78 (2016).

[8] B. Su, Y. Tian, and L. Jiang, J. Am. Chem. Soc. **138**, 1727 (2016).

[9] H. Sirringhaus, T. Kawase, R. Friend, T. Shimoda, M. Inbasekaran, W. Wu, and E. Woo, Science **290**, 2123 (2000).

[10] V. Bahadur and S. V. Garimella, Microelectron. J **39**, 957 (2008).

[11] R. Seemann, M. Brinkmann, T. Pfohl, and S. Herminghaus, Rep. Prog. Phys. **75**, 016601 (2012).

[12] S. D. Iliev and N. C. Pesheva, Langmuir **19**, 9923 (2003).

[13] S. Brandon, N. Haimovich, E. Yeger, and A. Marmur, J. Colloid Interface Sci. **263**, 237 (2003).

[14] C. Ishino, K. Okumura, and D. Quéré, Europhys. Lett. **68**, 419 (2004).

[15] H. Kusumaatmaja and J. M. Yeomans, Langmuir **23**, 6019 (2007).

[16] C. Schäfle, M. Brinkmann, C. Bechinger, P. Leiderer, and R. Lipowsky, Langmuir **26**, 11878 (2010).

[17] H. P. Jansen, K. Sotthewes, C. Ganser, C. Teichert, H. J. Zandvliet, and E. S. Kooij, Langmuir **28**, 13137 (2012).

[18] S. Ghosh, R. Lagraauw, S. Otten, A. Pit, C. Berendsen, J. Zeegers, D. Van Den Ende, and F. Mugele, Nat. Commun. **5**, 3559 (2014).

[19] G. Pashos, G. Kokkoris, and A. G. Boudouvis, Langmuir **31**, 3059 (2015).

[20] H. Kusumaatmaja, J. Chem. Phys **142**, 124112 (2015).

[21] W. Ren, Langmuir **30**, 2879 (2014).

[22] S. Varagnolo, V. Schiocchet, D. Ferraro, M. Pierno, G. Mistura, M. Sbragaglia, A. Gupta, and G. Amati, Langmuir **30**, 2401 (2014).

[23] J. Carmeliet, L. Chen, Q. Kang, and D. Derome, Langmuir **33**, 6192 (2017).

[24] Y. Wang, M. Jian, H. Liu, and X. Zhang, Langmuir **35**, 4387 (2018).

[25] Y. Wu, F. Wang, M. Selzer, and B. Nestler, Langmuir **35**, 8500 (2019).

[26] A. Cassie and S. Baxter, J. Chem. Soc. Faraday Trans. **40**, 546 (1944).

[27] See Supplemental Material at http://link.aps.org/supplemental/10.1103/PhysRevE.100.041102 for details of the calculation of the total interfacial energy, the numerical method, the choice of the initial states of droplets, and the validation of the high-symmetry property of equilibrated droplets.

[28] B. Nestler, F. Wendler, M. Selzer, B. Stinner, and H. Garcke, Phys. Rev. E **78**, 011604 (2008).

[29] H. Garcke, B. Nestler, B. Stinner, and F. Wendler, Math. Models Methods Appl. Sci. **18**, 1347 (2008).

[30] M. Ben Said, M. Selzer, B. Nestler, D. Braun, C. Greiner, and H. Garcke, Langmuir **30**, 4033 (2014).

[31] K. Schweigler, M. Ben Said, S. Seifritz, M. Selzer, and B. Nestler, Int. J. Heat Mass Transfer **105**, 655 (2017).

[32] D. Jacqmin, J. Fluid Mech. **402**, 57 (2000).

[33] A. Carlson, M. Do-Quang, and G. Amberg, Phys. Fluids **21**, 121701 (2009).

[34] E. Ueda, F. L. Geyer, V. Nedashkivska, and P. A. Levkin, Lab Chip **12**, 5218 (2012).

[35] W. Feng, L. Li, E. Ueda, J. Li, S. Heißler, A. Welle, O. Trapp, and P. A. Levkin, Adv. Mater. Interfaces **1**, 1400269 (2014).